

Assignment of chiral vectors in carbon nanotubesCh. Kramberger,¹ R. Pfeiffer,¹ H. Kuzmany,¹ V. Zólyomi,² and J. Kürti²¹*Institut für Materialphysik, Universität Wien, Strudlhofgasse 4, A-1090 Wien, Austria*²*Department of Biological Physics, Eötvös University Budapest, Pázmány Péter sétány 1/A, H-1117 Budapest, Hungary*

(Received 1 July 2003; revised manuscript received 15 September 2003; published 9 December 2003)

Double-wall carbon nanotubes were derived from peapods by annealing at high temperature. We report on the Raman response of the radial breathing mode (RBM) of the inner tubes. As a consequence of their small diameter the Raman spectra of these tubes show well distinguishable lines, besides the usual broad response from the outer tubes. An algorithm was developed to find the best (n, m) assignment for the observed lines. As a result of the assignment, we received $\nu_{\text{RBM}} = 233/d + 14$, ν_{RBM} in cm^{-1} for the ν versus $1/d$ relation, where d is the tube diameter in nm. To bring the discrepancy between calculation of RBM frequencies and experiment to a minimum, the diameters were evaluated from density functional theory.

DOI: 10.1103/PhysRevB.68.235404

PACS number(s): 81.07.De, 78.30.Na, 81.05.Tp

Due to their unique physical properties, carbon nanotubes (CNTs) have been of growing interest since their discovery in 1991.¹ Especially the interior of nanotubes opens a wide field of filling and confined nanochemistry. Particular attention must be paid at this point to the discovery² and filling^{3,4} of single-wall carbon nanotubes (SWCNTs).^{5,6} Filling the SWCNTs with various fullerenes developed the new carbon phases now known as “peapods.” Further on, the transformation of C_{60} inside a SWCNT into another thinner SWCNT was reported several times in recent years,^{7–9} and stimulated extensive interest in the scientific community. These so formed double-wall CNTs (DWCNTs) are an interesting material and especially the inner CNTs are of major interest. The latter have much smaller diameters (down to 0.5 nm) than CNTs produced in any other common way, such as laser ablation, CVD, arc discharge, or the HiPco process. Furthermore, they are synthesized in a chemically pure carbon environment. There is no catalyst needed and they were demonstrated to be of perfect purity without any further purification steps.⁹ Each of these inner CNTs has a well defined environment given by the surrounding outer CNTs. The DWCNTs were studied with high resolution Raman spectroscopy. The RBM response of the inner CNTs was found to exhibit extremely narrow line widths down to 0.35 cm^{-1} , confirming the extremely pure and defect free nature of this material. Additionally, the narrow RBM lines of the very thin CNTs are spread over a wide spectral range since the RBM frequency scales as the inverse diameter $1/d$ derived from

$$\nu_{\text{RBM}} = C_1/d + C_2, \quad (1)$$

where C_1 and C_2 are constants. On the other hand, for the narrow tubes the distance between RBM frequencies of geometrically allowed tubes is large enough to have their Raman response appearing as separated lines. Thus, DWCNTs provide an excellent material for the assignment of chiral vectors. The assignment of chiral vectors to experimental results of SWCNTs has been attempted several times. Raman scattering from individual tubes,^{10,11} luminescence from debundled tubes in solution, in combination with Raman scattering,¹² or even Raman scattering from DWCNTs Ref. 9 were used.

In this paper we present a detailed analysis of the Raman response of DWCNTs and describe an algorithm how such results can be used to assign chiral vectors to the Raman lines in detail. Correlations to reported results and caveats are discussed.

Peapods as well as pristine CNTs, both prepared in the form of bucky paper as described previously,¹³ were used as starting material. DWCNTs were obtained by annealing the peapods in a dynamic vacuum better than 5×10^{-7} mbar at 1280°C for 2 h. The sample was kept in the furnace while slowly cooling down.

The Raman spectra were recorded by a xy triple monochromator spectrometer from Dilor. The spectrometer can operate in additive and subtractive modes for high and normal dispersions, respectively. Each spectrum was recorded twice, once in the normal dispersion mode and additionally in the high dispersion mode. The samples were mounted inside a target cell with a dynamic vacuum better than 10^{-6} mbar. A copper cooling tip allowed to cool the samples down to either 90 K with liquid N_2 or 20 K with liquid He. All measurements were done in 180° backscattering geometry through the front window of the cell. An Ar/Kr laser, a He/Ne laser, and a tunable Ti:sapphire laser, pumped by an Ar laser, were used for excitation with 18 different laser lines.

The Gaussian diameter distribution of the pristine CNTs is centered at 1.39(2) nm with a standard deviation of 0.1 nm, and the filling of the peapods was found to be close to 100% by analysis according to work published previously in Refs. 14 and 15.

The RBM response of the inner CNTs arises after annealing. It is located above 200 cm^{-1} and shows many more distinguishable features than observed for the outer CNTs below 200 cm^{-1} .⁹ Figure 1 gives an example. The high dispersion mode of the spectrometer and lower temperatures reveal even more structure in the RBM of the inner NT.

The narrow RBM lines and their sparse distribution are a unique property of DWCNTs. Looking at the spectra recorded with normal resolution one is tempted to assign each peak to a particular tube species according to Eq. (1). The Raman cross section of a CNT changes dramatically with the excitation energy. In one particular spectrum only a selection of the CNTs is visible. By combining all spectra of the RBM

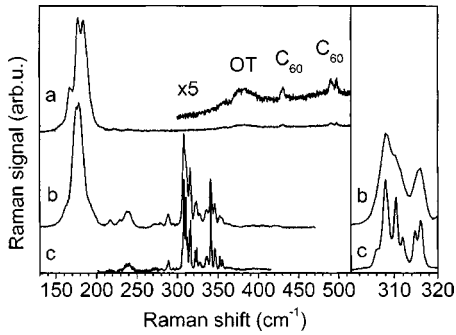


FIG. 1. Raman spectra of peapods recorded for 90 K and 515 nm excitation in normal resolution (a) and recorded for DWCNTs at 20 K and 568 nm in normal resolution (b) and high resolution (c). The right hand side shows a frequency blow up. OT means overtone of outer shell RBM.

in normal resolution and taking into account experimental errors of up to 1 cm^{-1} , we obtained a set of 39 mean line positions, ranging from 250 to 460 cm^{-1} . This counting does not consider splitting of the lines. A listing of these lines is presented in Table I. The table contains *all* observed lines down to a level of 1% of the strongest observed lines, with two exceptions at 360 and 380 cm^{-1} . These two lines are assigned to overtones of the outer CNT RBM response.

The distances between the geometrically allowed diameters are not uniform. They exhibit a distinct pattern. This pattern is expected to reappear in the sequence of line positions observed for the RBM. Since Eq. (1) is a monotone function, the ordering of the inverse diameters is the same as the ordering of their related RBM frequencies. An algorithm was developed to find the assignment that matches this pattern best. C_1 was limited to 210 and $250 \text{ cm}^{-1} \text{ nm}$, which covers well the values reported in the literature, and C_2 was set to 15 cm^{-1} . According to these limits and the observed spectral range of RBM frequencies (in our case 246 – 462 cm^{-1}) 52 different chiralities with diameters between 1.06 and 0.47 nm are candidates for this assignment. With these assumptions every possible assignment corresponds to a binary list of 52 elements. In the present case there are 37 identified RBM lines. That means the list consists of 37 “1” and 15 “0.” The binary representation of Table I starts, e.g., 11011. As the (10,4) CNT corresponds to “0” it is skipped. The (9,5) CNT corresponds to the third “1” in the sequence, so it is assigned to the third observed Raman line. More generally speaking, the p th “1” on position q denotes that the q th NT is assigned to the p th observed RBM line. New assignments can be obtained from existing ones by transposition of an arbitrary pair of “1” and “0.” As a consequence of this transposition the assignment between the selected elements move one step up or one step down. The better an assignment is the better the fit of C_1 with a constant value of C_2 matches to the pairs of assigned (inverse) diameter and frequency. The algorithm starts with a set of randomly generated assignments. The steps are (i) extending the set with new assignments generated by successive transposition and (ii) selecting a new subset of assignments with a smaller RMS. The solution is found by repeating (i) and (ii) until there are no longer any changes for

TABLE I. Inner shell SWCNT RBM frequencies and tube diameters: (1) center of gravity line position of the RBM (averaged from excitation with several lasers), (2) complete list of NTs, (3) interpolated DFT diameters, (4) first and second tight binding transition energies with $\gamma_0 = 2.9 \text{ eV}$, (5) theoretical RBM frequencies with $C_1 = 233 \text{ cm}^{-1} \text{ nm}$, $C_2 = 14 \text{ cm}^{-1}$, and $d = d_{\text{DFT}}$. “n.i.” means not identified.

ν_{RBM} expt. (cm^{-1})	Chirality (m,n)	d_{DFT} (nm)	E_{11}/E_{22} (eV)	ν_{RBM} theor.
246.1	(11,3)	0.997	0.84/1.59	247.8
252.4	(12,1)	0.978	0.86/1.60	252.1
n.i.	(10,4)	0.975	2.36/4.21	252.9
257.6	(9,5)	0.960	0.84/1.73	256.8
260.5	(8,6)	0.950	0.87/1.69	259.2
n.i.	(11,2)	0.947	2.40/4.24	260
n.i.	(7,7)	0.947	2.52/4.54	260
n.i.	(12,0)	0.937	2.40/4.25	262.6
265.3	(10,3)	0.921	0.87/1.84	267
270.5	(11,1)	0.901	0.85/1.91	272.5
274.7	(9,4)	0.901	0.82/1.75	272.5
n.i.	(8,5)	0.888	2.61/4.60	276.5
280.2	(7,6)	0.881	0.93/1.85	278.5
282.3	(10,2)	0.871	0.97/1.78	281.6
284.0	(11,0)	0.860	0.98/1.80	284.9
289.1	(9,3)	0.846	2.67/4.63	289.4
296.1	(8,4)	0.828	0.98/2.00	295.4
298.9	(10,1)	0.824	2.70/4.65	296.7
301.9	(7,5)	0.817	1.01/1.95	299.2
304.0 ^a	(6,6)	0.813	2.90/5.02	300.5
306.5	(9,2)	0.794	1.01/2.15	307.3
311.7	(10,0)	0.783	1.02/2.22	311.6
317.2	(8,3)	0.771	1.09/2.02	316.1
319.8	(7,4)	0.756	3.00/5.07	322.5
323.0	(9,1)	0.748	1.13/2.05	325.8
327.9	(6,5)	0.748	1.09/2.17	325.8
336.7	(8,2)	0.719	3.06/5.09	338.3
340.3	(9,0)	0.706	3.08/5.10	344.1
345.8	(7,3)	0.697	1.15/2.41	348.2
353.8	(6,4)	0.684	1.21/2.30	354.6
358.5	(5,5)	0.680	3.37/5.52	356.8
364.9	(8,1)	0.671	1.19/2.60	361.4
374.5	(7,2)	0.643	1.32/2.38	376.3
383.5	(8,0)	0.629	1.36/2.40	384.4
389.3	(6,3)	0.624	3.52/5.54	387.3
395.6	(5,4)	0.615	1.33/2.63	393.2
405.8	(7,1)	0.595	3.58/5.55	405.9
422.0	(6,2)	0.569	1.40/3.00	423.8
432.9	(7,0)	0.553	1.43/3.22	435.7
438.1	(5,3)	0.553	1.52/2.79	435.7
444.5	(4,4)	0.547	4.10/5.80	439.9
462.1	(6,1)	0.519	1.66/2.87	463.1

^aThis line is only observed in the high resolution mode.

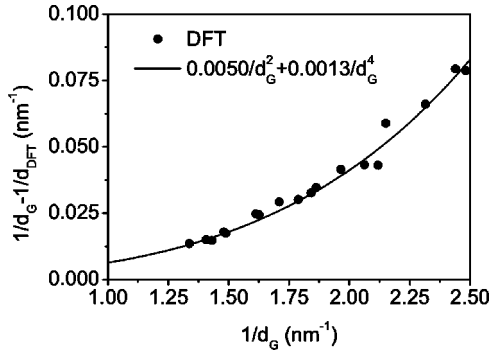


FIG. 2. Difference between graphene derived and DFT derived (inverse) diameters (bullets). The full drawn line is a polynomial interpolation.

consecutive cycles. Only these assumptions and rules are needed to reproduce the assignment or to create an assignment from any other set of experimental data. The averaged frequencies of the RBM lines and the assigned chiral vectors as determined from the algorithm described above are listed in Table I. Finally C_1 and C_2 were simultaneously fitted to the set of experimentally observed lines. The obtained values are $233 \text{ cm}^{-1} \text{ nm}$ for C_1 and 14 cm^{-1} for C_2 .

In the procedure described above the diameters of the nanotubes were used as evaluated from density functional theory (DFT) (for small enough unit cells) and a polynomial interpolation. For the calculation the Vienna Ab initio Simulation Package (VASP) was used as described previously.¹⁶ Figure 2 shows a plot of the deviation between diameters from the tight binding model and DFT optimized diameters for some very thin CNTs with unitcells up to 200 carbons. In order to obtain a correction for all diameters the data points were replaced by a smooth function.

$$1/d_{\text{DFT}} = 1/d_G - (0.0050/d_G^2 + 0.0013/d_G^4)$$

$$\text{with } d_G = 0.141 \sqrt{3(m^2 + mn + n^2)} / \pi. \quad (2)$$

Even though for the smallest assigned diameters the effect is only 2%, it is definitely noticeable (8 cm^{-1} of 400 cm^{-1}) and must be taken into account.

Even for the recording with normal resolution, the number of different Raman lines read out from the full set of spectra is much larger than the ones listed in Table I. There is definitely no way to assign different chiralities to all observed lines without an unreasonable high value for C_1 of more than $300 \text{ cm}^{-1} \text{ nm}$. The alternative explanation is that the RBM lines of the inner CNTs exhibit a splitting, as it was suggested in Ref. 9 and as it is suggestive from Fig 1. This splitting is not relevant for the presented analysis. Therefore the lines listed in Table I are the center of gravity value for each line pattern.

In the assignment presented in Table I metallic CNTs are included. According to the tight binding model such tubes have their first optical transition beyond the visible spectral range at least for the main body of Table I. Therefore they should not show up in the spectra recorded with visible light. However, for an assignment without any metallic CNT again an unreasonable value for C_1 of more than $300 \text{ cm}^{-1} \text{ nm}$

would be needed. Thus, the visibility of the metallic tubes is accepted and assumed to be a consequence of the breakdown of the tight binding model for the narrow tubes. DFT calculations show that considerable structure can appear in the joint density of states of metallic tubes, even below the first transition energy E_{11}^M .⁹ Alternatively or in addition, electronic inter tube transitions could have non-negligible matrix elements and could contribute to a resonance scattering. Deviations from the tight binding results are expected in particular for the very narrow tubes.

The assignment presented in this paper was obtained in a well defined and reproducible way. For very low RBM frequencies (large inner shell) the assignment cannot be confirmed directly. At line positions below 300 cm^{-1} the observed deviations between the fit frequencies and the experimentally observed frequencies reach a value equal to the differences between RBM frequencies of successive geometrically allowed CNTs. Therefore, it is evident that line positions located below 300 cm^{-1} can match a wide variety of different assignments, even though the whole assignment given here is reliable because the low frequency part is an immediate consequence of the assignment of the more narrow tubes.

Another crucial point for an unambiguous assignment is the completeness of the observed sequence of RBM lines. This was investigated by randomly skipping a few observed frequencies and running the algorithm with the remaining lines. Our findings are that incomplete sets of frequencies can lead to a large variety of independent assignments. Such assignments do not show a significant difference in the RMS ($< 5\%$).

The assignment by Jorio and co-workers in Refs. 10 and 11 is based upon Raman spectroscopy (line position and resonance enhancement) on as grown individual SWCNTs. The observed mean diameter in these experiments was about 1.3 nm . $\nu_{\text{RBM}} = C_1/d$ was used instead of Eq. (1). Therefore, a value of $C_1 = 248 \text{ cm}^{-1} \text{ nm}$ was obtained. Considering diameters between 1.1 and 1.5 nm and linewidths of $3-5 \text{ cm}^{-1}$, as reported in Ref. 11, there is no noticeable difference between the two expressions for the RBM frequency. Although the predicted frequencies of the RBM modes are in good agreement, this assignment cannot be compared directly to the assignment given here because the spectral ranges do not overlap.

The assignment published in Ref. 12 is an assignment of chiral vectors to optical transitions in individual HiPco CNTs. Some chiralities were also assigned to RBM frequencies. The observed Raman line positions overlap to some extent with the positions presented in Table I. Excellent agreement within 1 cm^{-1} is observed for these frequencies. Nevertheless, the same RBM lines are assigned to different chiralities. Figures 3 and 4 show fits for C_1 and C_2 to the linear relation between frequencies and assigned inverse diameters from Eq. (1). Figure 3 depicts the fit for the data in Table I (bullets). For comparison the fit to the data and assignment from Ref. 12 is also shown (triangles). The smaller RMS deviation looks suggestive on a first glance to favor the assignment represented by the triangles. This conclusion is misleading since in the latter case the number and density of

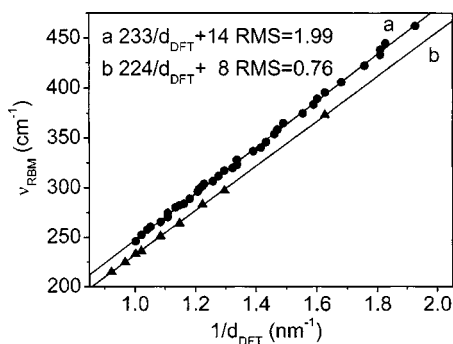


FIG. 3. Linear fits for Eq. (1) according to Table I (bullets) and Ref. 12 (triangles).

observed frequencies is much lower. Lower frequencies and less dense distributed frequencies render many more chances to find a suitable CNT for a given frequency. Therefore, the RMS deviation can only be used to compare different assignments for one set of line positions, but it is not appropriate for a comparison of assignments made upon different sets of line positions. Figure 4 shows the fits for the original assignment of Ref. 12 and an alternative assignment with exactly the same line positions. This figure clearly depicts the difficulty in unambiguously assigning chiral vectors to sparse sets of line positions.

Summarizing, the Raman response of double-wall carbon nanotubes prepared by annealing peapod precursors was found to exhibit very narrow and well distinguishable lines

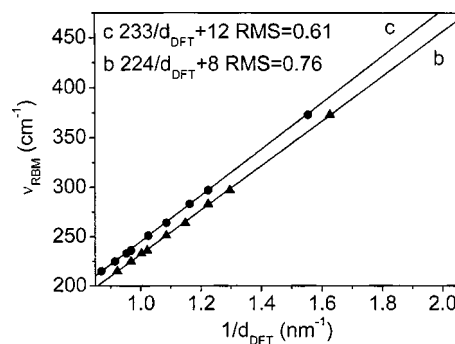


FIG. 4. Linear fits for Eq. (1) according to Ref. 12 (triangles) and an alternative assignment of the same line positions in Ref. 12, (bullets).

for the RBM of the inner shell tubes. As the distinguishable lines originate from different chiralities they can be unambiguously assigned to them. The crucial requirements for an unambiguous assignment are (i) a complete or nearly complete observation of the RBM frequencies of all geometrically allowed tubes, and (ii) the fact that this observation must be carried out for a diameter range where the lines can be addressed individually.

This work was supported by the FWF in Austria, Project 14893, by INTAS 00-237 and by OTKA T038014 in Hungary. The receipt of peapod samples from H. Kataura, Tokyo Metropolitan University, is gratefully acknowledged.

¹S. Iijima, *Nature (London)* **354**, 56 (1991).

²S. Iijima and T. Ichihashi, *Nature (London)* **363**, 603 (1993).

³J. Sloan, R. E. Dunin-Borkowski, J. L. Hutchison, K. S. Coleman, V. C. Williams, J. B. Claridge, A. P. E. York, C. Xu, S. R. Bailey, G. Brown, S. Friedrichs, and M. L. H. Green, *Chem. Phys. Lett.* **316**, 191 (2000).

⁴B. W. Smith, M. Monthieux, and D. E. Luzzi, *Nature (London)* **396**, 323 (1998).

⁵B. W. Smith and D. E. Luzzi, *Chem. Phys. Lett.* **321**, 169 (2000).

⁶H. Kataura, Y. Maniwa, T. Kodama, K. Kikuchi, K. Hirahara, K. Suenaga, S. Iijima, S. Suzuki, Y. Achiba, and W. Krätschmer, *Synth. Met.* **121**, 1195 (2001).

⁷S. Bandow, M. Takizawa, K. Hirahara, M. Yudasaka, and S. Iijima, *Chem. Phys. Lett.* **337**, 48 (2001).

⁸S. Bandow, G. Chen, G. U. Sumanasekera, R. Gupta, M. Yudasaka, S. Iijima, and P. C. Eklund, *Phys. Rev. B* **66**, 075416 (2002).

⁹R. Pfeiffer, H. Kuzmany, Ch. Kramberger, Ch. Schaman, T. Pichler, H. Kataura, Y. Achiba, J. Kürti, and V. Zólyomi, *Phys.*

Rev. Lett. **90**, 225501 (2003).

¹⁰M. S. Dresselhaus, G. Dresselhaus, A. Jorio, A. G. Souza Filho, Ge. G. Samsonidze, and R. Saito, *J. Nanosci. Nanotechnol.* **3**, 19 (2003).

¹¹A. Jorio, J. H. Hafner, C. M. Lieber, M. Hunter, T. McClure, G. Dresselhaus, and M. S. Dresselhaus, *Phys. Rev. Lett.* **86**, 1118 (2001).

¹²S. M. Bachilo, M. S. Strano, C. Kittrell, R. H. Hauge, R. E. Smalley, and R. B. Weisman, *Science* **298**, 2361 (2002).

¹³K. Hirahara, K. Suenaga, S. Bandow, H. Kato, T. Okazaki, H. Shinohara, and S. Iijima, *Phys. Rev. Lett.* **85**, 5384 (2000).

¹⁴H. Kuzmany, W. Plank, M. Hulman, Ch. Kramberger, A. Grüneis, Th. Pichler, H. Peterlik, H. Kataura, and Y. Achiba, *Eur. Phys. J. B* **22**, 307 (2001).

¹⁵H. Kuzmany, R. Pfeiffer, C. Kramberger, T. Pichler, X. Liu, M. Knupfer, J. Fink, H. Kataura, Y. Achiba, B. W. Smith, and D. E. Luzzi, *Appl. Phys. A: Mater. Sci. Process.* **76**, 449 (2003).

¹⁶J. Kürti, G. Kresse, and H. Kuzmany, *Phys. Rev. B* **58**, R8869 (1998).